Using a digital camera as a measuring device

Salvador Gil[a)]
Escuela de Ciencia y Tecnología, Universidad Nacional de San Martín, Provincia de Buenos Aires, Argentina 1653 and Departamento de Física, "J. J. Giambiagi"-Facultad de Ciencias Exactas y Naturales, Universidad de Buenos Aires, Argentina 1428

Hernán D. Reisin
Departamento de Física, "J. J. Giambiagi"-Facultad de Ciencias Exactas y Naturales, Universidad de Buenos Aires, Argentina 1428

Eduardo E. Rodríguez
Departamento de Física, "J. J. Giambiagi"-Facultad de Ciencias Exactas y Naturales, Universidad de Buenos Aires, Argentina 1428 and Departamento de Física y Química, Facultad de Ingeniería y Ciencias Exactas y Naturales, Universidad Favaloro, Buenos Aires, Argentina

(Received 26 October 2005; accepted 12 May 2006)

We present several experiments that can be done using a digital camera or a webcam, including the shapes of shadows cast by lampshades, the trajectories of water jets, the profile of a hanging chain, and caustic figures produced by the reflection of light on mirrors of different forms. The experiments allow for a simple and direct quantitative comparison between theory and experiment. © *2006 American Association of Physics Teachers.*
[DOI: 10.1119/1.2210487]

I. INTRODUCTION

The main objective of this paper is to discuss a variety of instructive experiments that can be done using a low cost digital camera (or webcam). The experiments are either novel or the setup is new. Those that have been done previously with a different experimental setup have been reformulated. The associated theory ranges from elementary topics in mechanics and the ray theory for light to more advanced subjects that require the solution of differential equations.

We first discuss the shapes of shadows produced by a lampshade on a wall. This activity is used to illustrate the general approach that is used in the other projects, that is, take photographs of physical phenomena and compare them with the corresponding theoretical predictions. We then discuss the trajectory of projectiles in two dimensions, an easy arrangement to explore the shape of a hanging chain supported at its extremes when it is subjected to different loading, how to build a simple and inexpensive device to explore the relation between an arbitrary shaped mirror and its corresponding reflection caustic figure, and suggest a number of other applications of a digital camera that can be done using similar experimental techniques, such as the study of beam deflection and Chladni plate figures.

Some of these phenomena are not commonly discussed in introductory textbooks, although they are understandable to undergraduate students. We have implemented them so that they can be easily studied in a more quantitative manner, using the advantages of digitized images. The projects discussed here require a resolution of 480×640 pixels or better and a modest personal computer, and may be particularly useful to schools and universities with modest experimental facilities. Most new digital cameras also allow the generation of short movies at rates of 15 and 30 frames per second (fps). In this way it is possible to record the position of objects at different times, which is particularly useful for studying the kinematics of objects. This use constitutes an alternative to stroboscopic photography and time exposure techniques. This useful feature of digital cameras will not be discussed in the present work.[1–3]

II. EXPERIMENTAL PROCEDURE

We follow a common procedure for all the experiments, which is to digitally record and analyze the data acquired in two-dimensional (2D) images. The procedure works for any experiment where the relevant physical features are entirely contained in a single plane of the photograph. Care must be taken to obtain photographs with a minimum of distortion by ensuring that the camera is parallel and along (or close to) the normal to the plane that defines the figure of interest; the distance of the camera to the object of interest should be much larger than the characteristic dimension of the object. If the camera has a zoom, pin cushion and barrel distortions[4] are minimized when the zoom is set about halfway between wide (W) and telephoto (T).[5]

It is convenient to place vertical and horizontal scales with easily identifiable marks in the same plane as the object of interest. An alternative is to use a grid of known dimensions in the background that is coincident or close to the plane of the object being studied and perpendicular to the axis of the camera. In this way each photograph records all the necessary information to convert the pixel coordinates of the digital photograph into a real coordinate system. There are several ways to perform this transformation. A straightforward way is to use a graphics program, such as PHOTOEDITOR or COREL DRAW. By placing the mouse on the reference scale, it is simple to convert from pixel coordinates to real dimensions. There are also several commercial[1–3] and shareware[6] programs that can directly convert the pixel coordinates of the picture into real coordinates. Alternatively, it is possible to write a spreadsheet program so that by clicking on a digital image imported into the program, the pixel coordinate will be given in the spreadsheet. Another possibility is to trim the digital image to a well-known real size and then create a graph with the same dimensions. Importing the trimmed digital image into the plot area of this graph will automatically produce a plot in real coordinates. This approach allows for a direct comparison of the model and the actual data. This technique has been used by one of the au-

thors to quantitatively study the Bernoulli equation in the drainage of vessels.[7]

III. CHARACTERIZING THE GEOMETRY OF A SHADOW

The shadows cast by a lampshade can present regular and interesting patterns. Recently, Horst[8] discussed this problem using a visual method to characterize the shape of the shadow. The light emerging from a lampshade forms a cone, with the vertex at the position of the light bulb filament and an angular aperture defined by the rim of the lampshade. Depending on the orientation of the axis of the light cone relative to the wall, we expect to observe a shadow with hyperbolic, parabolic, or other conical shapes. By using a digital photograph it is possible to quantitatively test this expectation.

Once the coordinates of the shadow are known, it is straightforward to compare the results with the corresponding theoretical prediction. In Figs. 1(a) and 1(b) we show the case where generatrix of the light cone is parallel to the wall. We create this condition by inclining the lamp so that the edge of the shadow on the ceiling is right above the lamp. In this case the shape of the shadow on the wall is fitted using a parabola. By visually comparing the overlap of the theoretical curve with the rim of the shadow, we can extract the relevant parameters of the model (in this case the coefficients of the quadratic).[9] In Fig. 1(c) the axis of the light cone is parallel to the wall. The expected shape of the shadow is a hyperbola that results from the intersection of the light cone with the wall. We can superpose onto the digital image the result of the model developed in Ref. 8.

IV. THE TRAJECTORY OF A WATER JET FROM A HOSE

Our setup is similar, but simpler than an earlier arrangement that required a system to generate and shoot drops of water, in combination with stroboscopic light.[10] In our setup a nozzle is introduced to discharge the water and the hose is directly connected to a faucet. With a little practice it is easy to obtain a uniform jet of water. It is important to maintain the flow of water so that the initial velocity v_0 of the jet is constant. While one student maintains the exit nozzle at a fixed angle, another student takes a picture of the trajectory of the jet. It is convenient that the complete trajectory of the jet is captured by a single frame so that it contains all the useful information about the system: the initial angle, maximum height, range, and shape of the trajectory. We used a background grid of 20 cm $\times$ 20 cm to provide a convenient reference scale.

If the effect of friction air is negligible, the trajectory can be described by the equation of motion of a projectile,

$$y(x) = y_0 + \tan\,\theta_0(x - x_0) - \frac{g}{2v_0^2\cos^2\,\theta_0}(x - x_0)^2, \qquad (1)$$

where (x_0, y_0) are the coordinates of the exit of the nozzle, θ_0 and v_0 are the initial angle and speed of the jet, and g represents the gravitational field, which is antiparallel to the y axis. The range $x_{\max}$ and the maximum height $y_{\max}$ of the jet are $x_{\max} = v_0^2 \sin(2\theta_0)/2g$ and $y_{\max} = v_0^2 \sin^2\,\theta_0/2g$, so that $y_{\max}/x_{\max} = \frac{1}{2}\tan\,\theta_0$. Therefore, the ratio of the maximum height to the range characterizes the initial angle of the jet. If

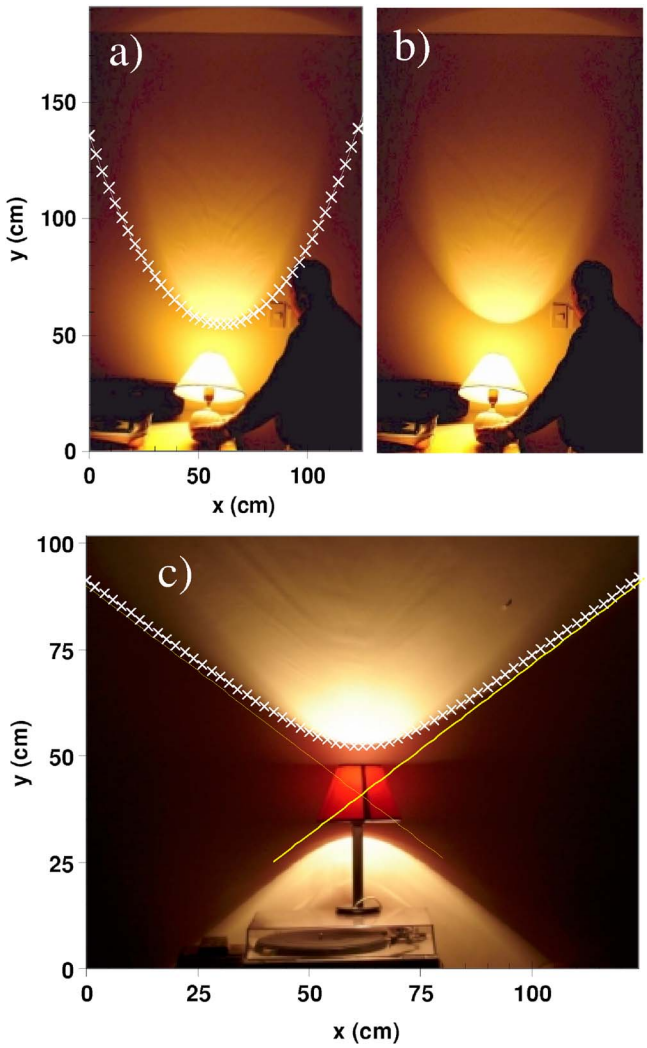

Fig. 1. (a) and (b). Shadow cast by a lampshade on the wall when the generatrix of the cone of light is parallel to the wall. (a) The crosses are the theoretical expectation of the shadow and (b) the photograph of the shadow. (c) Shadow cast by a lampshade on the wall, with the axis of the lamp (and its cone of light) parallel to the wall. The continuous lines represent the asymptotes of the hyperbola fitted to the shadow. The crosses denote the theoretical hyperbola that best fits the shape of the shadow.

we vary the initial velocity v_0, it is simple to fit the actual trajectory of the jet to Eq. (1). In Fig. 2 we give an example of this analysis. In our case variations of a few percent in the value of v_0 produce noticeable discrepancies between the actual trajectory and the theoretical prediction. The value of v_0 can be determined with an uncertainty of about 4%. Near the nozzle we observe a well-defined jet of water, whereas far from the nozzle, the jet breaks into drops of different sizes. Nonetheless, the jet and the drops follow the same trajectory. This observation may be useful for confronting students with the misconception that liquids and solids follow different laws of physics.[7]

The value of v_0 can be compared with an independent measurement of the velocity obtained by measurements of the water flux, that is, the time it takes the hose to fill a known volume. Because the exit area A of the nozzle can be measured directly, the value of v_0 can be obtained from the flux of water, $Q = Av_0$. We found that the values of v_0 obtained by these two methods agree within a few percent.

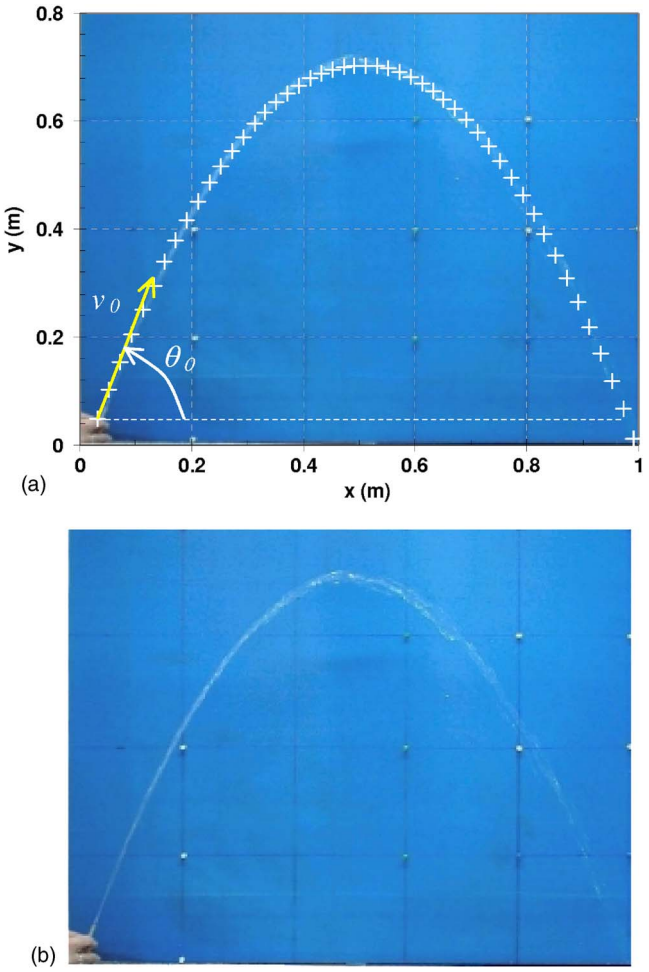

Fig. 2. Trajectory of a water jet. (a) The digital image superposed on the prediction according to Eq. (1), represented by crosses. The parameters v_0 and θ_0 can be obtained from the fit to the actual trajectory; (b) plain photograph of the jet.

The fact that the observed trajectory and the theoretical prediction, Eq. (1), coincide indicates that the effect of air friction can be disregarded in this case.

V. CATENARIES

The shapes of hanging chains have intrigued many scientists. Galileo claimed, erroneously, that this shape was a parabola. Leibniz, Huygens and Johann Bernoulli seem to have solved this problem in response to a challenge by Jakob Bernoulli in 1691.[13] We call this curve a catenary (from the Latin word for chain). Its solution can be found in many textbooks.[11] In Appendix A we reproduce a simple justification and highlight the ideas used in determining the shape of a catenary.

For a chain of length L_c with uniform mass density hanging from two points located at the same height h and separated by a distance L in a uniform gravitational field, the catenary is given by

$$y(x) = \frac{1}{\lambda}(\cosh(\lambda x) - 1), \tag{2}$$

where λ can be found by solving

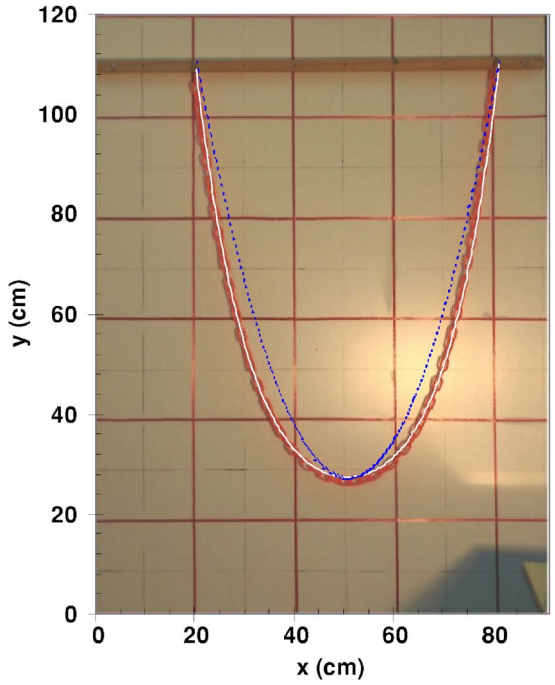

Fig. 3. Superposition of the image of a hanging chain and the prediction (heavy continuous line) given by Eqs. (2) and (3). For comparison we show the parabola (dashed lines) that goes through the vertex and hanging points. We see that the catenary describes the shape of the chain more precisely.

$$\frac{\lambda L_c}{2(\lambda h + 1)} = \tanh(\lambda L/2). \tag{3}$$

In Fig. 3 we show the digital image of a chain and the catenary obtained using Eqs. (2) and (3). For comparison, we also show the shape of the parabola that has the same vertex and the same hanging points. The catenary clearly gives a much better description of the actual shape.

In Fig. 4 we show the image of a uniformly loaded chain. Here the loads (150 g each) were uniformly distributed horizontally (x axis) on a 125-g chain, so that mass per unit of horizontal length, $dm/dx \approx$ const. Also shown is the catenary and a parabola. In this case the parabola gives a better description of the shape of the chain, in agreement with theory (see Appendix A). This situation can also be tested on actual hanging bridges[12] and used to test the theory for the shape of nonuniform cables.[13]

The forces along the hanging chain (loaded or unloaded) are pure tensile forces because the chain cannot support any compression due to its flexibility. If the system were flipped, all the forces due to weight would be reversed and the curve along the chain would be subject to pure compression forces. Because many traditional construction materials, such as bricks and stone, can withstand great compression but small tensile forces, the catenary would make a perfect arch using these types of materials. The same idea can be used for designing a loaded arch. The famous Catalan architect Antoni Gaudi used this principle to design some of the beautiful and astonishing structures he built in Barcelona.

VI. REFLECTION CAUSTICS

When we observe a cup of white tea or coffee, we often see an illuminated heart-like figure, particularly if there is a

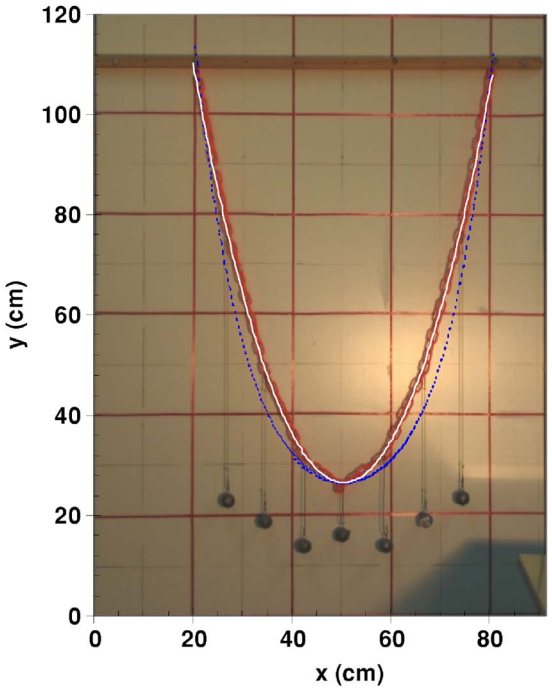

Fig. 4. Image of a uniformly loaded chain. The heavy line is a parabola and the dashed line is a catenary. The parabola gives a better description of the shape of this chain.

single light source illuminating the cup obliquely from above. This same figure can be observed inside a gold ring[14,15] under the same illumination conditions. These figures are examples of the caustic figures produced by the envelope of the rays reflected from the circular surface of the cup or the ring (see Fig. 5). Many great scientists have worked on this interesting problem, including Huygens and Bernoulli.[16,17]

It is possible to find the form of the caustic for any type of reflecting curve. If a beam of horizontal parallel rays shines onto the surface of a concave reflecting surface described by $y=f(x)$, it can be shown that the parametric equations for the caustics, produced by a light source located at $x\rightarrow-\infty$, are[18] (see Appendix B)

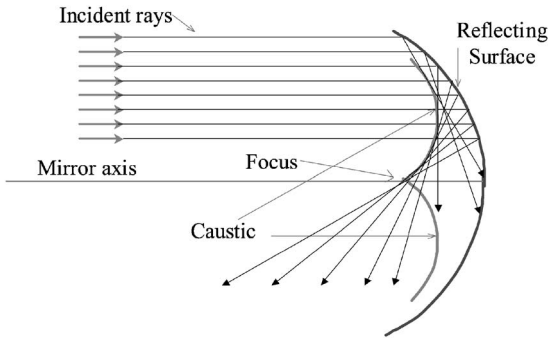

Fig. 5. Schematic of the formation of the caustic (catacaustic). The envelope of the reflected rays is the caustic of the reflecting surface. The region enclosed between the caustic and the reflecting surface is enhanced as a result of the superposition of incident and reflected rays that pass through this space.

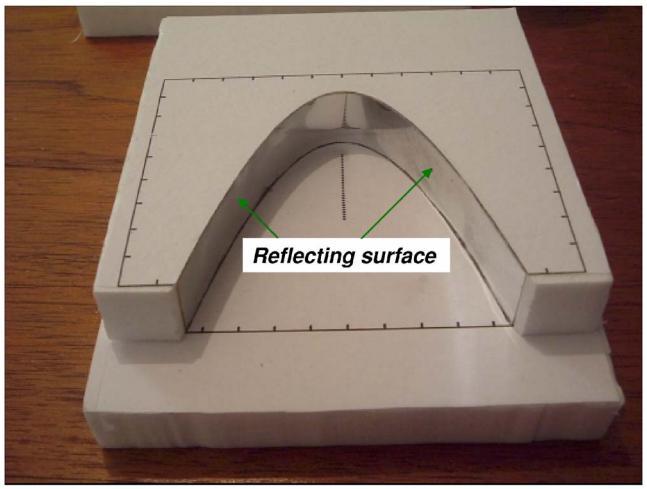

Fig. 6. Schematic of the experimental arrangement for building a mirror with a given shape.

$$\begin{cases} y_c(t) = f(t) + \dfrac{(f'(t))^2}{f''(t)}, \\ x_c(t) = t + \dfrac{f'(t)[1-(f'(t))^2]}{2f''(t)} \end{cases} . \tag{4}$$

The experimental setup is illustrated in Fig. 6. We drew the profiles of differently shaped mirrors on paper using a one-to-one scale. Then we glued this plot to an expanded polycarbonate slab, 0.75 in. Then we carefully cut the silhouette of the curve out of the plate, with a thin hot wire (heated by an electrical current) using the plot as a reference. A strip of aluminized Mylar, about 2 cm wide and 20 μm thick, was glued onto the wall.

In Fig. 7 we show the image of a circular mirror illuminated from the left. The image of the caustic is very clear. Overlapped on this image is the curve that describes the shape of the mirror and its corresponding caustic according to Eq. (4). The agreement between theory and observation is very good. We found that using the Sun as the light source produced the best results. In Fig. 8 we show the results for an exponential mirror and its caustic.

VII. BEAM DEFLECTION AND ELASTICA

The deflection of a beam is another interesting classical problem.[19] The case of small and large[20] transverse deflections of a horizontal beam, fixed at one end and subject to varying loading, is discussed in many textbooks on elasticity.[21] By taking digital photographs, it is possible to compare the shape of the beam for different loadings with theory.[20] The details of the theory have been discussed recently in Ref. 20. In Fig. 9 we present the case of large deflection of a plate. For this experiment we used a plate of high molecular weight, polystyrene, thickness 0.3 cm, width 3 cm, and length 40 cm. The shape of the plate can be readily compared with the theoretical curve, known as the elastica.[20] Figure 9 shows that the theoretical curve describes the observed deflection of the plate. The unknown parameter is the Young's modulus of the material which can be determined by overlapping the deformed material with the best theoretical fit.

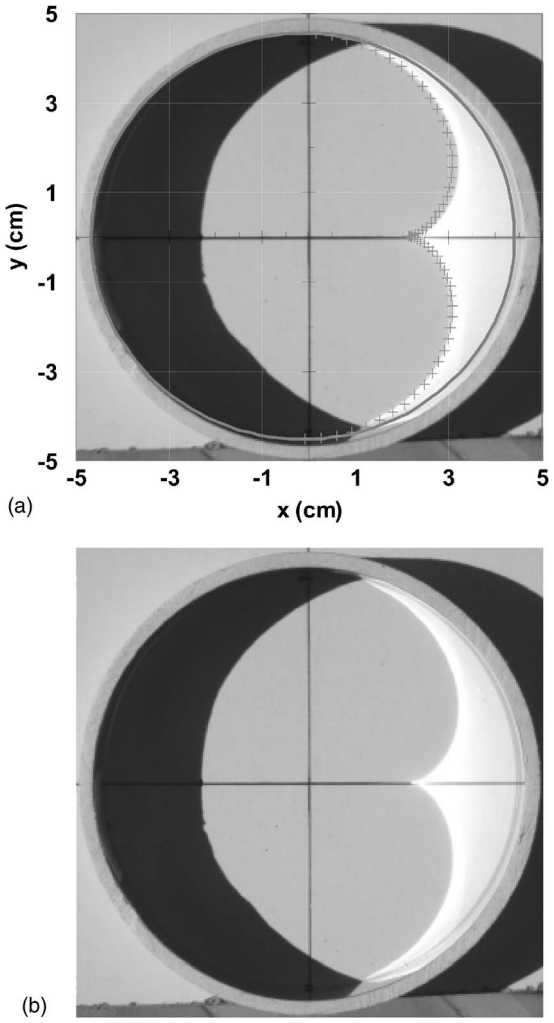

Fig. 7. (a) Superposition of the caustic for a circular mirror (catacaustic) and the theoretical prediction given by Eq. (4); (b) photograph of the phenomenon.

VIII. OTHER PROJECTS

There are a number of other experiments that can profit from the advantages of a digital image for quantitative analysis and comparison with theory. For example, most students are familiar with nodes and antinodes in a vibrating string. The generalization of this idea to the vibration of a two-dimensional plate is relatively simple, where the nodes of the string are replaced by nodal curves. Spreading white sand on a vibrating plate can easily reveal these shapes. Sand accumulate along the nodal lines known as Chladni figures, which are produced at different resonance frequencies.[22,23] If we take a digital photograph of the patterns produced at each resonant frequency, it is possible to compare the experimental figures with theory. Recently this technique has been used to study the drop formation in a falling stream of liquid.[24] Other experiments that benefit from the use of a digital camera are interference and diffraction patterns produced by pinholes and slits. By using a solid state or a HeNe laser, it is easy to project the diffraction or interference pattern on a wall. If we take a digital photograph of the pattern, we can use software such as MAPLE OR MATHEMATICA to obtain the intensity along a line. We can then compare the intensity patterns with the corresponding theoretical models. A detailed description of this technique is in Ref. 25.

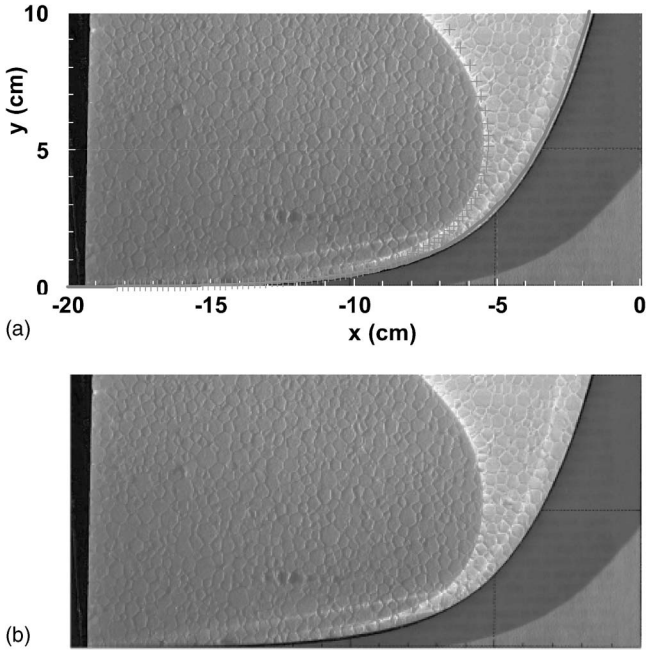

Fig. 8. (a) Superposition of the caustic for an exponential mirror and the theoretical prediction given by Eq. (4); (b) photograph of the phenomenon.

ACKNOWLEDGMENTS

We would like to express our acknowledgement to Dr. A. Schwint, E. Batista, and D. Di Gregorio for their careful reading of the manuscript and their useful suggestions.

APPENDIX A: CATENARY

We briefly review the assumptions that lead to the equation of the catenary. Consider a chain of length L_c and mass M_c suspended by its ends as indicated in Fig. 10. The weight of an infinitesimal element of length ds in a uniform gravi-

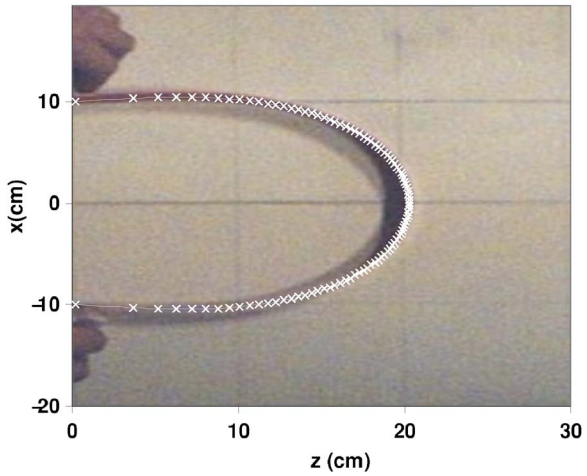

Fig. 9. Elastica of a flexible plastic strip of length L=51.2 cm. The theoretical curve obtained using the algorithm discussed in Ref. 20 describes the shape of the beam.

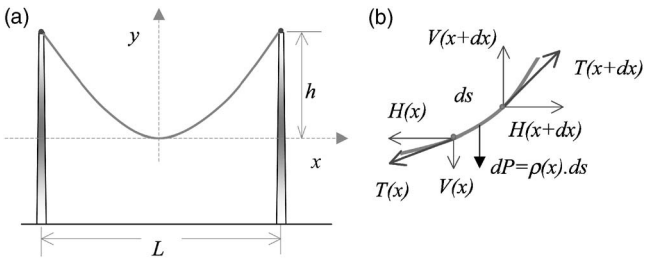

Fig. 10. (a) Chain or flexible rope suspended by its ends. The coordinates of the hanging points are $(-L_2,h)$ y (L_1,h), with $L_1+L_2=L$. (b) Forces that act on an infinitesimal element of chain of length ds.

tational field is $dP=\rho(x)g\,ds$, where g is the acceleration of gravity and $\rho(x)$ is the local mass density per unit of length of the chain. If $H(x)$ and $V(x)$ are the horizontal and vertical components of the tension of the chain at the point with coordinate x, the equilibrium of the forces along the x and y axes leads to

$$H(x+dx)=H(x)=H_0 \tag{A1}$$

and

$$V(x+dx)-V(x)=dV=dP=\rho(x)g\,ds, \tag{A2}$$

where H_0 represents the tension of the chain at the vertex (where $dy/dx=0$). The tension of the chain at the point with coordinate x is tangent to the curve $y(x)$ and thus

$$\frac{V(x)}{H(x)}=\frac{dy}{dx}. \tag{A3}$$

Equation (A3) is based on the physical condition that the chain is subject only to tensile forces. If we differentiate Eq. (A3) and combine it with Eqs. (A1) and (A2), we obtain

$$dV=\frac{d^2y}{dx^2}H_0dx=\rho(x)g\,ds. \tag{A4}$$

If $dm/dx=\rho(x)ds/dx=$const., it follows that the shape of the chain $y(x)$ is a pure parabola. This situation holds if on a chain of negligible weight, we hang masses that are uniformly distributed horizontally as in the example shown in Fig. 4 or in hanging bridges, where most of the weight is on the platform of the bridge. In general, this condition is not satisfied and Eq. (A4) must be solved explicitly for each function $\rho(x)$. Because $ds=dx\sqrt{1+(dy/dx)^2}$, we can write Eq. (A4) as

$$\frac{d^2y}{dx^2}=\lambda(x)\sqrt{1+\left(\frac{dy}{dx}\right)^2}, \tag{A5}$$

where $\lambda(x)=\rho(x)g/H_0$. Equation (A5) can be integrated by substituting $z(x)=dy/dx$,

$$\int^x\frac{dz}{\sqrt{1+z^2}}=\int^x\lambda(x')dx', \tag{A6}$$

which implies that

$$z=\left.\frac{dy}{dx}\right|_x=\sinh(u(x))+c_1, \tag{A7}$$

where $u(x)\equiv\int^x\lambda(x')dx'$. For constant mass density $\rho(x)=M_c/L_c$, $\lambda=M_cg/(H_0L_c)$ is a constant, and Eq. (A7) reduces to $dy/dx=\sinh(\lambda x)+c_1$. If we choose the origin to coincide with the vertex of the chain (where $dy/dx=0$), then $c_1=0$. The integration of Eq. (A7) yields $y(x)=1/\lambda\cosh(\lambda x)+c$. The condition $y(x=0)=0$ leads to

$$y(x)=\frac{1}{\lambda}(\cosh(\lambda x)-1). \tag{A8}$$

The constant λ can be obtained from the boundary conditions, namely the position of the ends with a chain length L_c. If the ends are at the same height h and separated by a distance L, then from Eq. (A8) we have

$$h=\frac{1}{\lambda}(\cosh(\lambda L/2)-1). \tag{A9}$$

The length of the chain is

$$L_C=2\int_0^{L/2}\sqrt{1+(dy/dx)^2}dx=\frac{2}{\lambda}\sinh(\lambda L/2). \tag{A10}$$

If we combine Eqs. (A8) and (A9), we obtain

$$\frac{\lambda L_c}{2(\lambda h+1)}=\tanh(\lambda L/2), \tag{A11}$$

which relates the parameters λ, L, L_c, and h.

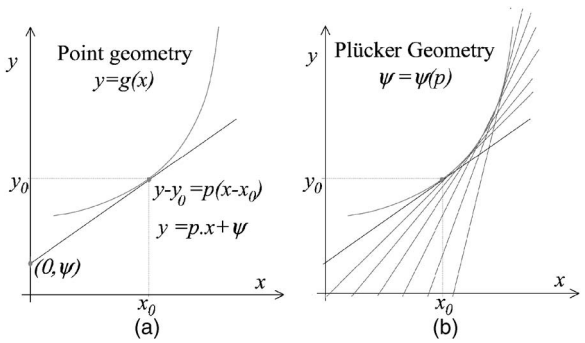

Fig. 11. By conventional point geometry, the curve is characterized by the relation $y=g(x)$. Equivalently, the same locus can be characterized by a set of tangent lines to the curve determined by the relation $\psi=\psi(p)$.

APPENDIX B: THE CAUSTIC

The caustic is the envelope of a family of rays transmitted (diacaustic) by a lens or reflected (catacaustic) by a mirror. We briefly summarize the relation between the shape of the caustic and the reflecting surface. There are several ways to obtain the equations of the caustic of a mirror.[14–17] We summarize the argument originally discussed in Ref. 18 based on the Legendre transformation.[26,27]

By means of conventional point geometry, a curve is characterized by the relation $y=g(x)$. Equivalently, a family of tangents to the curve can characterize the same curve (see Fig. 11). Because each line can be described by its slope p $[=dg(x)/dx]$ and the intersection ψ with the y axis, the relation $\psi=\psi(p)$ can be used to represent a family of tangents to the curve. This representation is known as the Plücker line geometry.[27] It can be shown that $y=g(x)$ and $\psi=\psi(p)$ are two equivalent representations of the curve.[27] From Fig. 11(a), it follows that

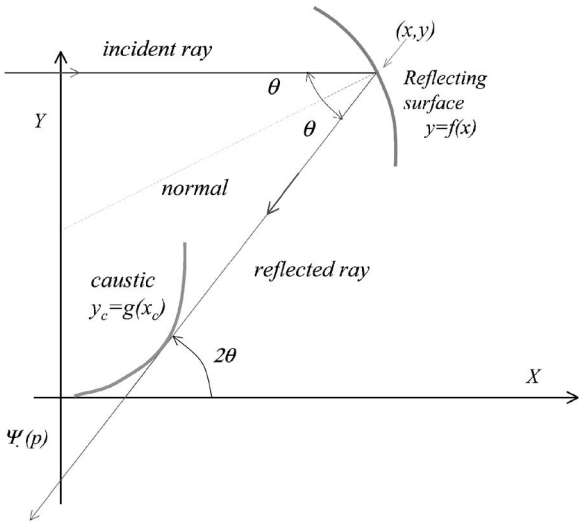

Fig. 12. Schematic of the relation between the reflecting surface, represented by $y=f(x)$ and the caustic characterized by $y_c(x_c)$. The incident rays come from a source on the far left.

$$p=\frac{(y_0-\psi)}{x_0}, \quad \text{or } \psi=y_0-px_0. \tag{B1}$$

Therefore, if we know the family of tangents expressed by $\psi=\psi(p)$, according to Eq. (B1) $\partial\psi/\partial p=-x$. The conventional point representation, $y=g(x)$, can be obtained from Eq. (B1),

$$y=g(x)=xp+\psi(p). \tag{B2}$$

This type of transformations is often used in mechanics when we go from the Lagrangian formulation to a Hamiltonian formulation.

Consider a concave reflecting surface characterized by $y=f(x)$ and a beam of horizontal parallel rays incident from the left (see Fig. 12). If θ is the angle of incidence on the mirror relative to the normal to the reflecting surface, then $\tan\theta=-1/f'(x)$. The slope of the reflected ray is $p=\tan(2\theta)$ and its intersection with the y axis is ψ. The equation of the reflected ray can be written as

$$Y-f(x)=p(X-x), \tag{B3}$$

where

$$p=\tan(2\theta)=2f'(x)/(1-(f'(x))^2), \tag{B4}$$

Y and X are the coordinates of any point on the reflected ray, and $(x,f(x))$ is the point of incidence of the incoming ray on the mirror. We can write

$$\psi(p)=Y(X=0)=f(x)-xp. \tag{B5}$$

Equation (B5) can be regarded as the expression of the family of tangent lines that characterize the locus of the caustics in Plücker line geometry.[18,27] To convert to the conventional point geometry of the caustic, $y_c=g(x_c)$, we can use the Legendre transformation

$$x_c=-d\psi/dp=(p-f'(x))\frac{dx}{dp}+x. \tag{B6}$$

We combine Eqs. (B4) and (B6) and obtain

$$x_c=\frac{f'(x)[1-(f'(x))^2]}{2f''(x)}+x. \tag{B7}$$

From Fig. 12 we can write

$$y_c=x_cp+\psi(x). \tag{B8}$$

If we replace Eqs. (B4), (B5), and (B7) in Eq. (B8), we have

$$y_c=\frac{(f'(x))^2}{f''(x)}+f(x). \tag{B9}$$

Therefore the parametric equations of the caustics are

$$y_c(x)=f(x)+\frac{(f'(x))^2}{f''(x)},$$

$$x_c(x)=x+\frac{f'(x)[1-(f'(x))^2]}{2f''(x)}. \tag{B10}$$

[a]Electronic mail: sgil@df.uba.ar

[1] LOGGER PRO 3 from Vernier software (www.vernier.com).
[2] VIDEOPOINT CAPTURE II (www.Pasco.com).
[3] A. Heck, "Coach: An environment where mathematics meets science and technology," in Proceedings of the ICTMT4, Plymouth, 1999, edited by W. Maull and J. Sharp (University of Plymouth, UK, 2000).
[4] E. Hecht, *Optics*, 2nd ed. (Addison-Wesley, Boston, MA, 1990).
[5] We thank one of the reviewers for pointing out this caveat.
[6] XYEXTRACT GRAPH DIGITIZER (http://www.gold-software.com/download5149.html).
[7] M. E. Saleta, D. Tobia, and S. Gil, "Experimental study of Bernoulli's equation with losses," Am. J. Phys. **73**(7), 598–602 (2005).
[8] K. E. Horst, "The shape of lamp shade shadows," Phys. Teach. **39**, 139–140 (2001).
[9] Examples of EXCEL files illustrating this procedure can be downloaded from www.fisicarecreativa.com. This site also describes experimental projects and reports of experiments performed by undergraduate students from Latin American universities.
[10] B. Tolar, "The water drop parabola," Phys. Teach. **18**, 371–372 (1980).
[11] M. R. Spiegel, *Theoretical Mechanics* (Schaum, NY, 1967), Chap. 7.
[12] Qualitative displays of these phenomena are shown in some science museums, for example, MateUBA, Buenos Aires (http://www.fcen.uba.ar/museomat/mateuba.htm).
[13] M. C. Fallis, "Hanging shapes of nonuniform cables," Am. J. Phys. **65**(2), 117–122 (1997).
[14] Ch. Ucke and C. Engelhardt, "Playing with caustic phenomena," in Proceedings of the GIREP/ICPE Conference on New Ways in Physics Teaching, Ljubljana, 21–27 August 1996, pp. 440–444.
[15] A. D. McIntosh, "An equation for the caustic curve," Phys. Educ. **25**, 171–173 (1990).
[16] Famous curves (http://turnbull.mcs.st-and.ac.uk/history/Curves/Curves.html).
[17] Eric W. Weisstein, *World of Mathematics* (CRC, Boca Raton, FL, 1999); (http://mathworld.wolfram.com/topics/CausticCurves.html); Eric W. Weisstein, "Caustic" (http:mathworld.wolfram.com/Caustic.html).
[18] C. Bellver-Cebreros and M. Rodriguez-Danta, "Caustics and the Legendre transform," Opt. Commun. **92**, 187–192 (1992).
[19] Th. Hopfl, D. Sander, and J. Kirshner, "Demonstration of different bending profiles of a cantilever caused by a torque or a force," Am. J. Phys. **68**, 1113–1115 (2001).
[20] A. Valiente, "An experiment in nonlinear beam theory," Am. J. Phys. **72**(8), 1008–1012 (2004).
[21] W. A. Nash, *Strength of Materials*, 2nd ed. (McGraw-Hill, NY, 1998).
[22] J. R. Comer, M. J. Shepard, P. N. Henriksen, and R. D. Ramsier, "Chladni plates revisited," Am. J. Phys. **72**(10), 1345–1346 (2004).

[23] T. D. Rossing, "Comment on 'Chladni plates revisited' by J. R. Comer, M. J. Shepard, P. N. Henriksen, and R. D. Ramsier [Am. J. Phys. **72**(10), 1345–1346 (2004)]," Am. J. Phys. **73**(3), 283 (2005).
[24] V. Grubelnik and M. Marhl, "Drop formation in a falling stream of liquid," Am. J. Phys. **63**(5), 415–419 (2005).
[25] G. Robert Wein, "A video technique for the quantitative analysis of the Poisson spot and other diffraction patterns," Am. J. Phys. **67**(3), 236–240 (1999).
[26] H. Goldstein, C. Poole, and J. Safko, *Classical Mechanics*, 3rd ed. (Addison-Wesley, Boston, MA, 2001).
[27] H. Callen, *Thermodynamics and an Introduction to Thermostatistics*, 2nd ed. (Wiley, NY, 1985).

Surveyor's Compass. The standard curriculum for American colleges in the middle of the 19th century almost always included a course on surveying. This surveyor's compass is marked "E.A. Kutz of New York" and is in the Greenslade Collection. Compasses of this type were used for rapid field work; they used peep-sights instead of a telescope and cross hairs, and the circles are divided into degrees, and not subdivided with a vernier scale. (Photograph and Notes by Thomas B. Greenslade, Jr., Kenyon College)